Science Advances

AAAS

advances.sciencemag.org/cgi/content/full/4/3/eaap9096/DC1

Supplementary Materials for

Dislocation-driven growth of two-dimensional lateral quantum-well superlattices

Wu Zhou, Yu-Yang Zhang, Jianyi Chen, Dongdong Li, Jiadong Zhou, Zheng Liu, Matthew F. Chisholm, Sokrates T. Pantelides, Kian Ping Loh

Published 23 March 2018, *Sci. Adv.* **4**, eaap9096 (2018)
DOI: 10.1126/sciadv.aap9096

The PDF file includes:

Other Supplementary Material for this manuscript includes the following:
(available at advances.sciencemag.org/cgi/content/full/4/3/eaap9096/DC1)

- movie S1 (.mp4 format). Scheme showing the dislocation climb and the corresponding quantum well growth process.

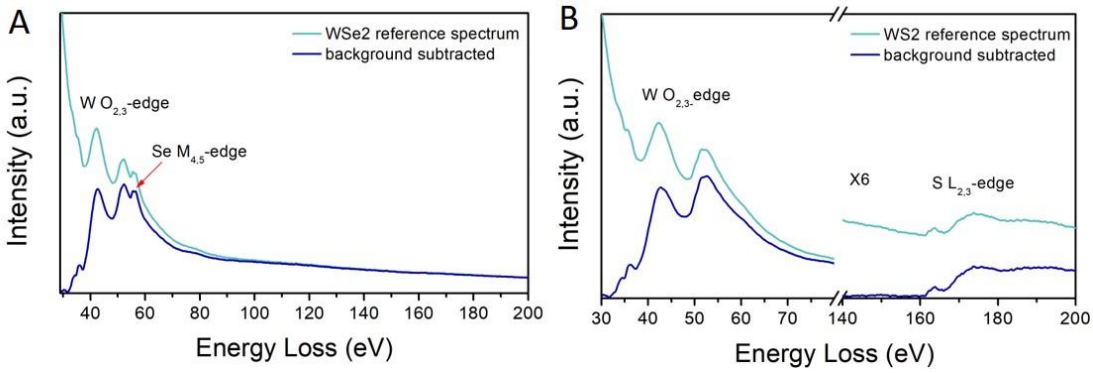

fig. S1. Reference EELS spectra from pure WSe_2 and WS_2 monolayers. Reference EELS spectra from pure WSe_2 (**A**) and WS_2 (**B**) monolayers.

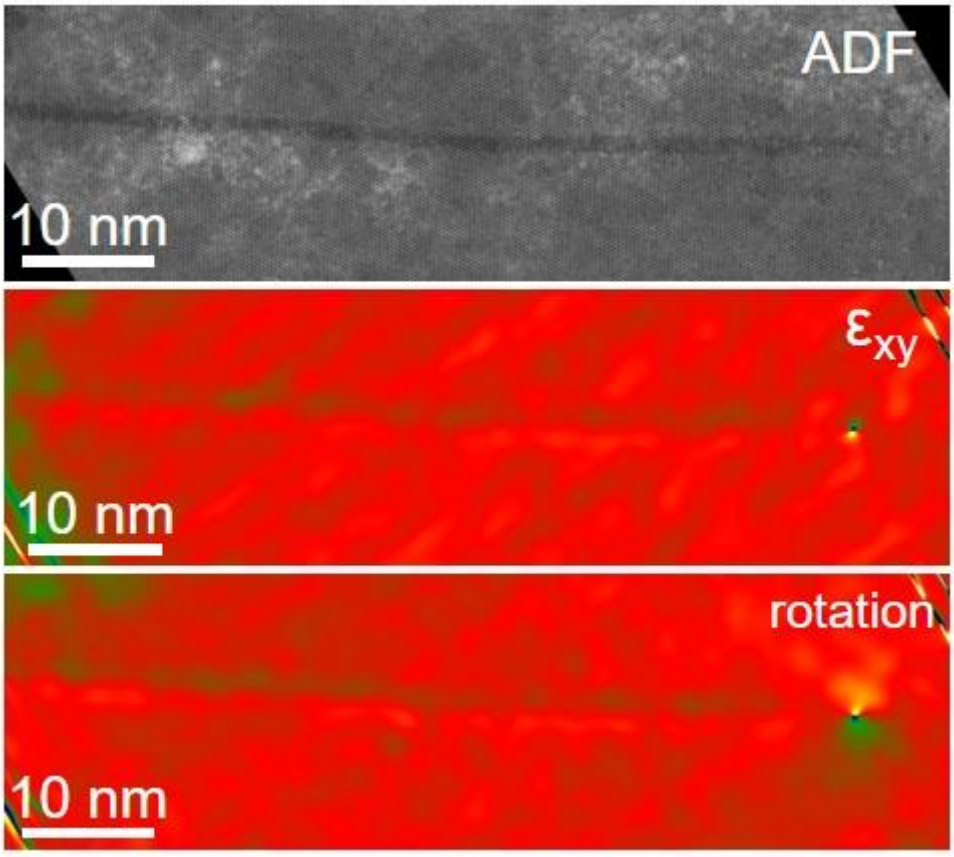

fig. S2. STEM-ADF of the entire 65-nm-long WS_2 quantum well and the corresponding strain distribution around the quantum well. The ADF image is the same as the one shown in Fig. 1F in the main text.

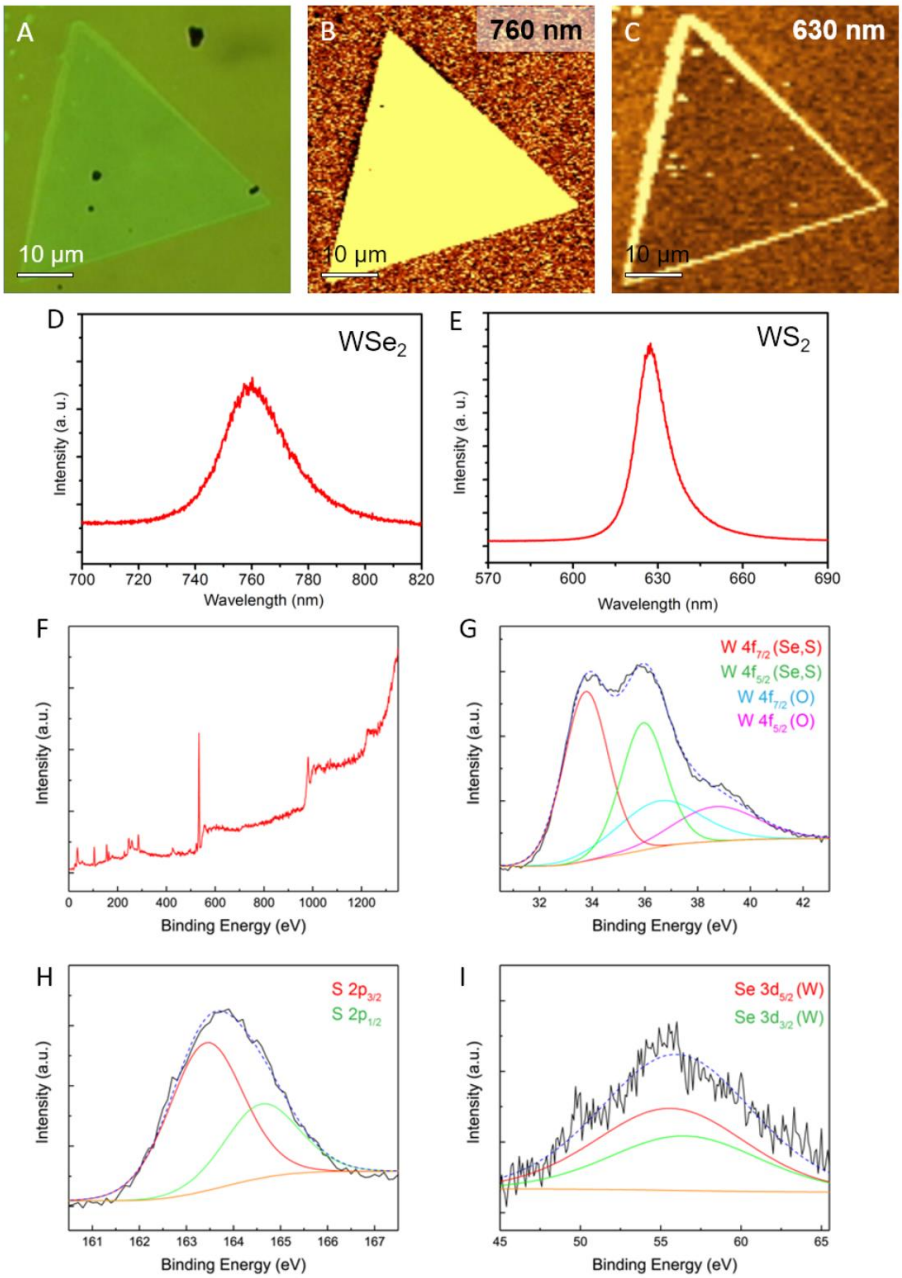

fig. S3. Optical images and spectroscopy measurements of the WSe_2/WS_2 lateral heterostructure. (**A**) Optical image of a WSe_2/WS_2 lateral heterostructure. (**B**) Photoluminescence (PL) intensity mapping at 760 nm showing the spatial distribution of the characteristic PL signals from WSe_2 monolayer. (**C**) PL intensity mapping at 630 nm showing the spatial distribution of the characteristic PL signals from WS_2 monolayer. (**D** and **E**) PL spectra of the WSe_2 core and WS_2 shell regions of the lateral heterostructure, respectively. (**F-I**) X-ray photoelectron spectroscopy (XPS) analysis of the WSe_2/WS_2 heterostructures showing (F) a full spectrum from 0 to 1380 eV, (G) W *4f*, (H) S *2p*, and (I) Se *3d* core levels, respectively. Characteristic W $4f_{7/2}$ and $4f_{5/2}$ peaks locating at ~33.8 (red) and 36.0 eV (green),

respectively, represent the W^{4+} states in WSe_2 and/or WS_2. In addition, characteristic W $4f_{7/2}$ and $4f_{5/2}$ peaks locating at ~36.7 (cyan) and 38.9 eV (pink), respectively, were also observed, representing the W^{6+} states in WO_3 precursor residuals. Characteristic Se $3d_{5/2}$ (red) and $3d_{3/2}$ (green) peaks locating at ~55.3 and 56.2 eV, respectively, represent the Se^{2-} states in WSe_2. Characteristic S $2p_{3/2}$ (red) and $2p_{1/2}$ (green) peaks locating at ~ 163.5 and 164.7 eV represent the S^{2-} states in WS_2.

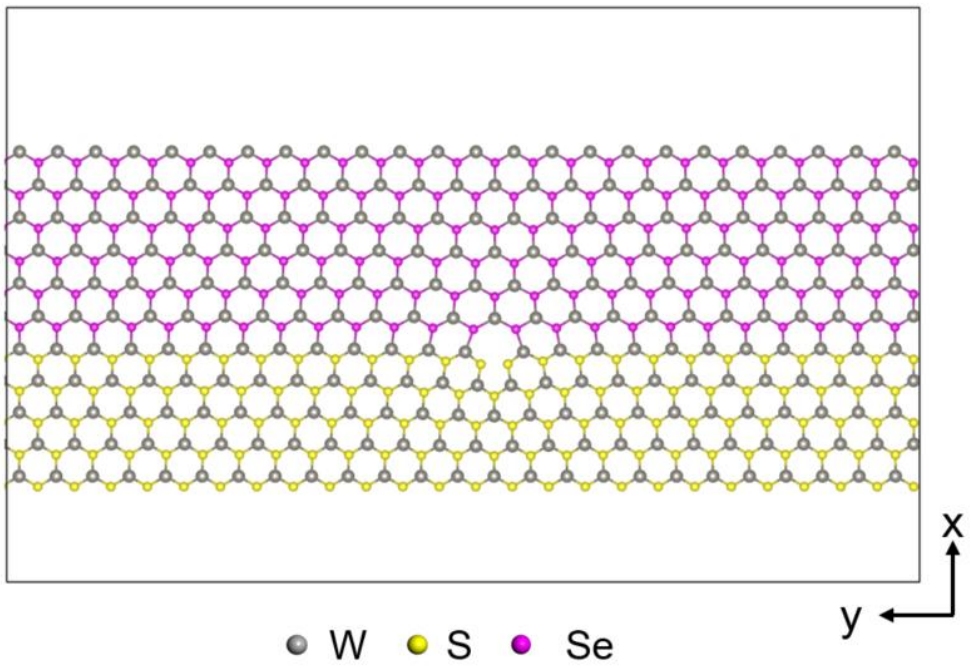

fig. S4. Atomic model of WSe_2/WS_2 heterostructure. Every 25 units of WS_2 (79.53 Å) match 24 units of WSe_2 (79.56 Å), resulting in a 5|7 dislocation to release the stress. Vacuum layer in the x- and z- directions is larger than 15Å.

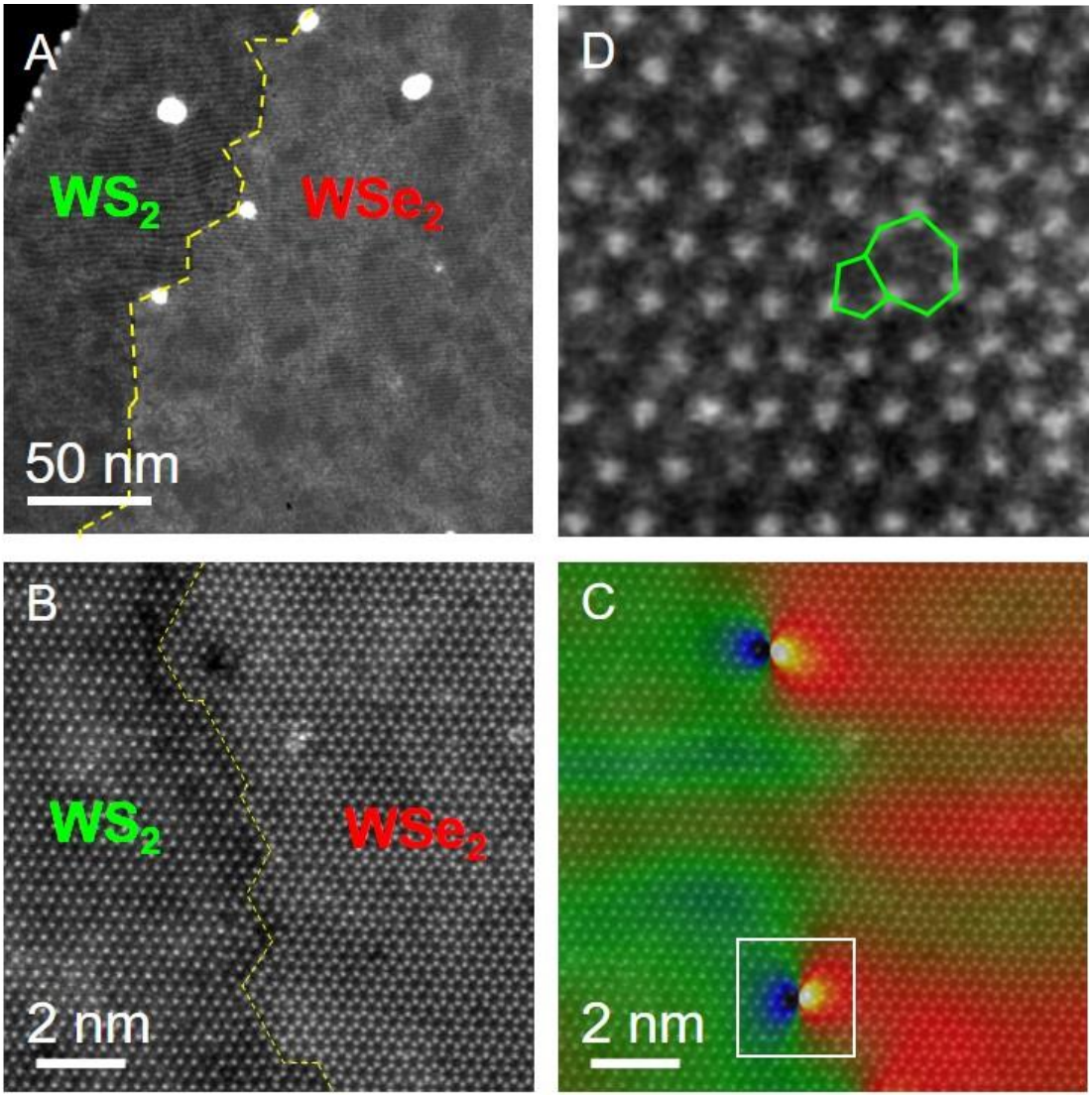

fig. S5. Additional structural characterization data from the lateral WSe_2/WS_2 heterointerface. (**A**) Low magnification STEM-ADF image of the WSe_2/WS_2 lateral interface without the formation of WS_2 quantum wells. The yellow dashed lines highlight the epitaxial interfaces. (**B**) Atomic-resolution STEM-ADF image of the WSe_2/WS_2 lateral interface. (**C**) The corresponding strain distribution, overlaid onto the ADF image, showing the formation of misfit dislocations that are ~8 nm apart. (**D**) A magnified view of the misfit dislocation, composing of 5|7 member rings, from the region highlighted in (C).

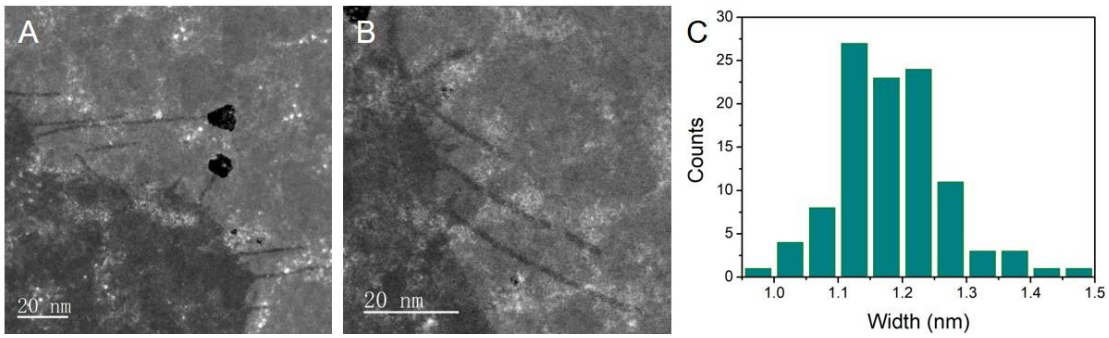

fig. S6. Additional low-magnification STEM-ADF images showing the formation of arrays of WS_2 quantum wells at the WSe_2/WS_2 lateral interface, driven by dislocations. The brighter regions are WSe_2 while the WS_2 monolayer regions show lower image intensity. (**C**) Width distribution of the WS_2 quantum wells. The average width of the WS_2 quantum wells in the WSe_2 monolayer is 1.19±0.09 nm, measured from 106 quantum wells.

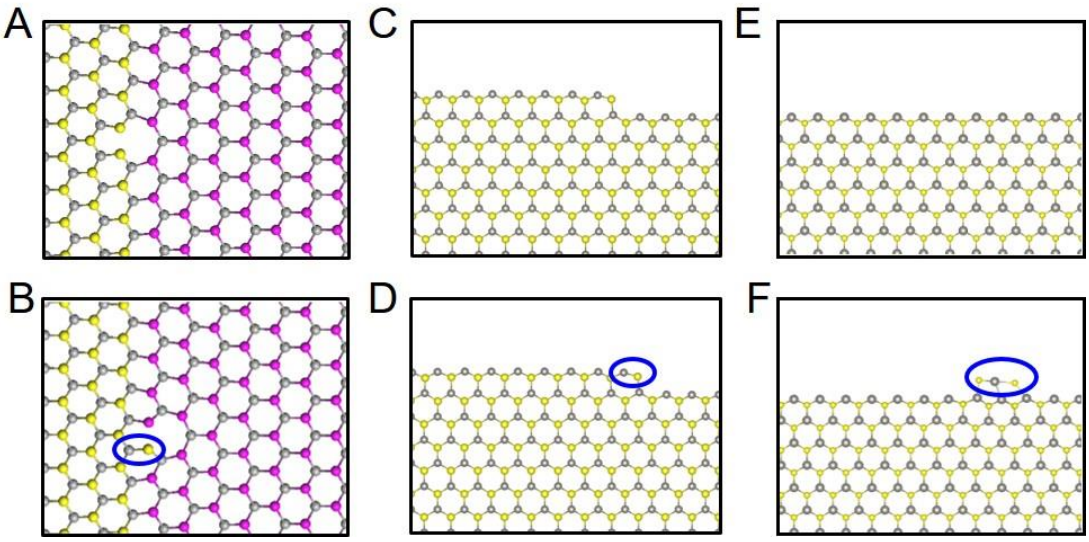

fig. S7. Comparison between dislocation climb and extension of a WS_2 edge during the sample growth. Atomic models of (**A**) WS_2/WSe_2 interface with a 5|7 dislocation, (**B**) insertion of a W-S_2 unit resulting in a dislocation climb, (**C**) WS_2 island with a W-terminated zigzag step edge, (**D**) extension of the step edge due to the adsorption of a W-S_2 unit, (**E**) WS_2 island with a W-terminated zigzag straight edge, and (**F**) growth of WS_2 island due to the adsorption of a W-S_2 unit. Newly inserted/adsorbed W-S_2 units are highlighted by the blue circles.

During the second step of the heterostructure growth, *i.e.* growth of WS_2, the source atoms (W and S) can either insert into a misfit dislocation core (dislocation climb) at the hetero-interface or attach to the fresh WS_2 edge (edge extension). We calculate the formation energy of this process. Formation energy E^f is defined as following: $E^f = E(new) - E(old) - \mu_W - 2 \times \mu_S$. E(old) and E(new) are the total energies before and after the insertion/adsorption, respectively. μ_W and μ_S are chemical potentials of W and S. Because the change of number of atoms are the same for insertion and adsorption, the choice of chemical potential does not affect the comparison of formation energy. For simplicity, we chose chemical potential from bulk materials.

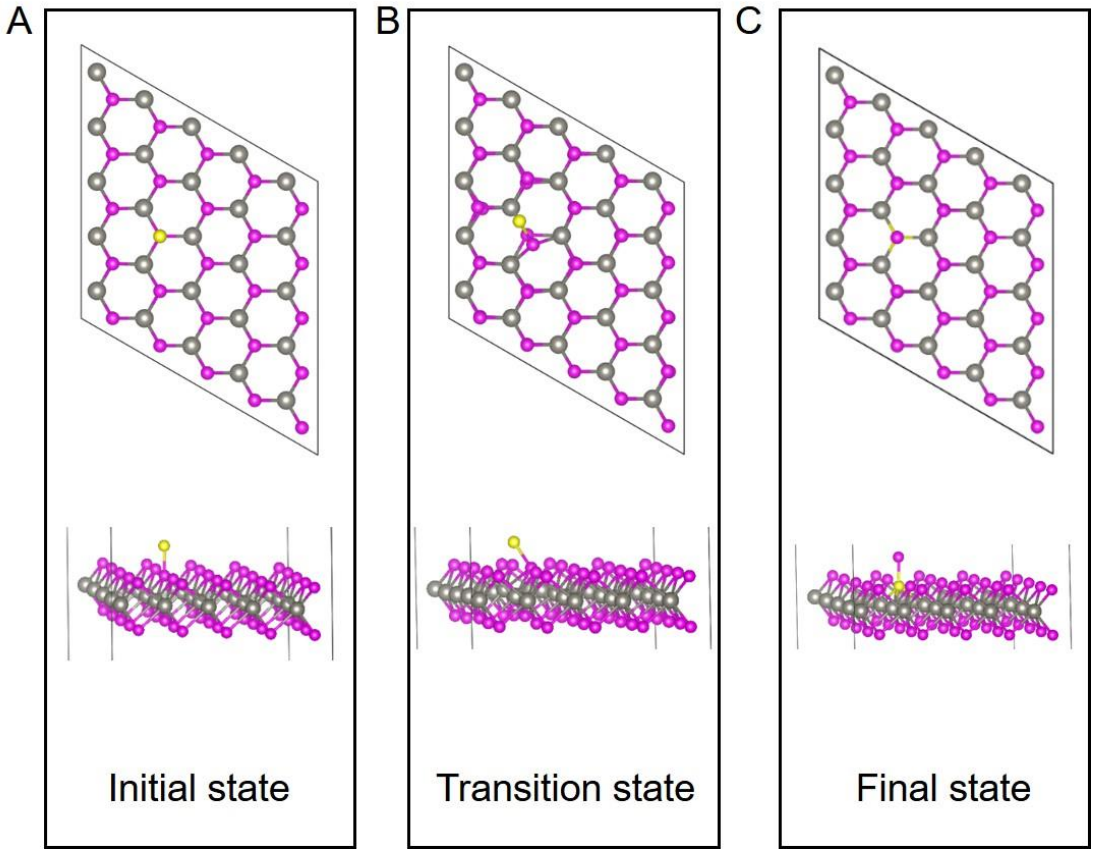

fig. S8. Atomic models for the S_{Se} substitution barrier calculations. (**A**) Optimized initial state, in which a S atom is on top of a Se atom. (**B**) Optimized transition state. (**C**) Optimized final state, in which Se atom is on top of a S atom. Top panels are top views and bottom panels are perspective views.

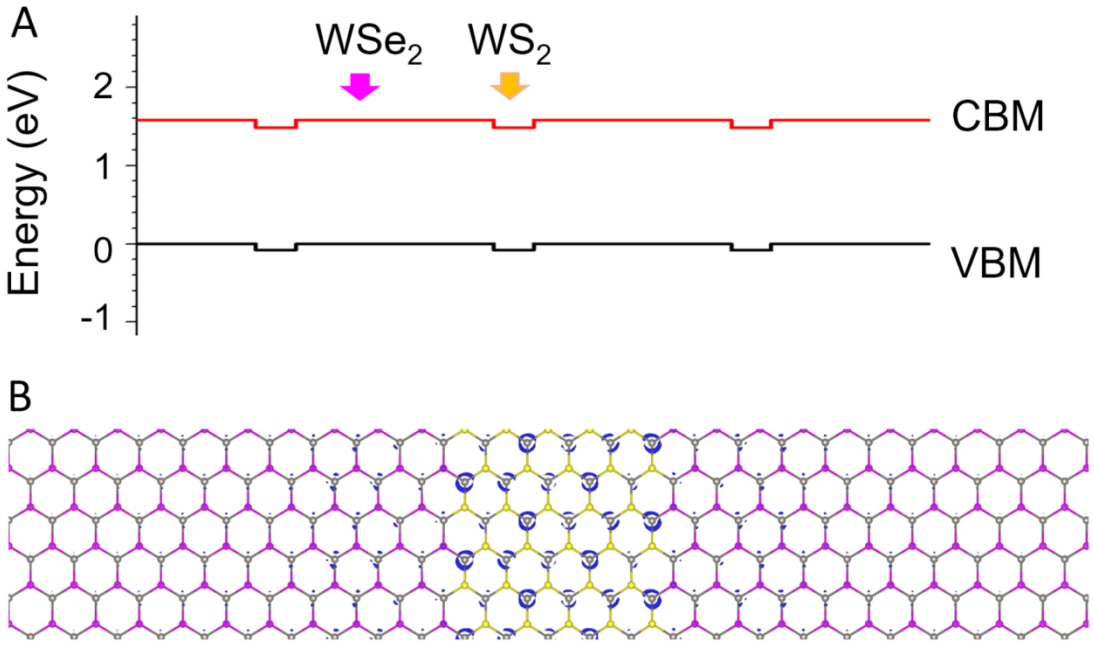

fig. S9. Band structure of lateral WSe_2/WS_2 superlattice. (**A**) Energy band alignment for the WSe_2/WS_2 superlattice calculated with PBE functional. Comparing with Fig. 4A, both HSE06 functional calculations and PBE functional calculations reveal a type-II band alignment. (**B**) Electron density difference between the system with an extra electron and the original charge neutral system, showing the modulation doping effect in a lateral WSe_2/WS_2 superlattice. The iso-surface with a value of 0.0015 e/Å^3 is shown in blue color. The extra electron mainly accumulates in the WS_2 region due to a type-II band alignment.

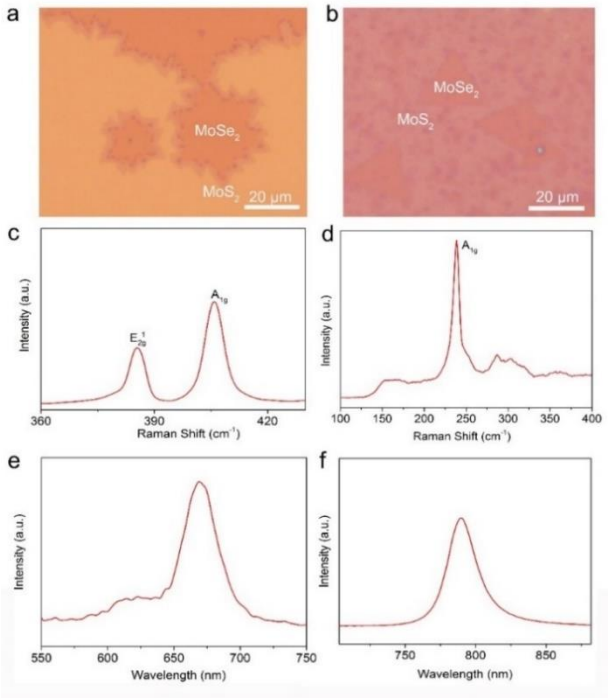

fig. S10. Optical images and spectroscopy measurements of the $MoSe_2/MoS_2$ lateral heterostructure. (**A** and **B**) Optical images of the $MoSe_2/MoS_2$ lateral heterostructure with different shapes, with monolayer $MoSe_2$ as the core and monolayer MoS_2 as the shell. (**C** and **E**) Raman and photoluminescence (PL) spectra of the shell region of the lateral heterostructure, conforming the shell is MoS_2 monolayer. (**D** and **F**) Raman and PL spectra of the core region of the lateral heterostructure, conforming the core is $MoSe_2$ monolayer.

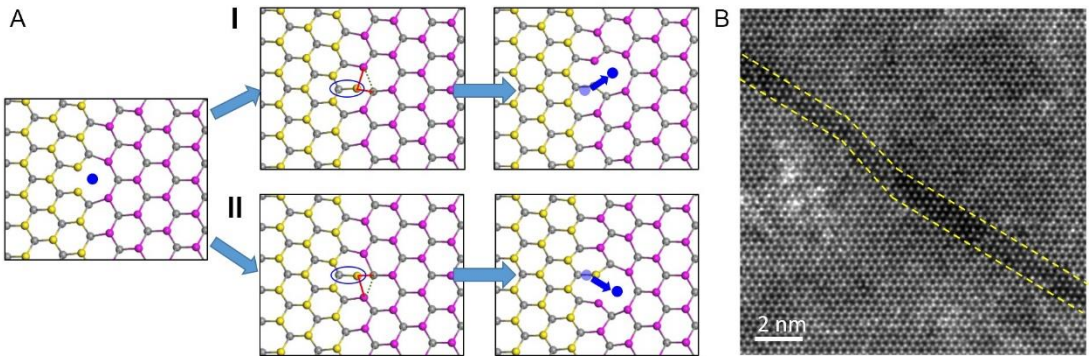

fig. S11. Dislocation climb and formation of nanosize kinks during the growth of quantum well. (**A**) Schematic of the dislocation climb. First a W-S_2 unit is inserted into the 5|7 dislocation core, followed by two types of bond reconfiguration **I** and **II**. The gray dashed lines illustrate the original bonds, while the red lines represent the new bonds. The blue circles highligh the inserted W-S_2 units. As a consequence of the bond reconfiguration, the dislocation climb has either a sidewise component (*i.e.* wiggling) upwards or downwards with respect to the armchair growth direction, as illustrated by the blue arrows where the blue dots highlight the positions of the new heptagons and the translucent dots represent the original positions of the heptagons. (**B**) STEM-ADF image showing the formation of a nano-size kink in the WS_2 quantum well. The formation of such kinks is due to the sidewise wiggling of dislocation climb during the growth of the quantum well.